Stability of Annexin V in Ternary Complexes with Ca^{2+} and Anionic Phospholipids: IR Studies of Monolayer and Bulk Phases†

Fangjun Wu,‡ Carol R. Flach,‡ Barbara A. Seaton,§ Tanya R. Mealy,§ and Richard Mendelsohn*,‡

Department of Chemistry, Newark College, Rutgers University, Newark, New Jersey 07102, and Department of Physiology, Boston University School of Medicine, 80 East Concord Street, Boston, Massachusetts 02118

Received August 17, 1998; Revised Manuscript Received November 12, 1998

ABSTRACT: Annexin V (AxV) is a member of a family of proteins that exhibit functionally relevant Ca^{2+}-dependent binding to anionic phospholipid membranes. Protein structure and stability as a function of Ca^{2+} and phospholipids was studied by bulk phase infrared (IR) spectroscopy and by IR reflection−absorption spectroscopy (IRRAS) of monolayers in situ at the air/water (A/W) interface. Bulk phase experiments revealed that AxV undergoes an irreversible thermal denaturation at ∼45−50 °C, as shown by the appearance of amide I bands at 1617 and 1682 cm^{-1}. However, some native secondary structure is retained, even at 60 °C, consistent with a partially unfolded "molten globule" state. Formation of the Ca^{2+}/phospholipid/protein ternary complex significantly protects the protein from thermal denaturation as compared to AxV alone, Ca^{2+}/AxV, or lipid/AxV mixtures. Stabilization of AxV secondary structure by a DMPA monolayer in the presence of Ca^{2+} was also observed by IRRAS. Spectra of an adsorbed AxV film in the presence or absence of Ca^{2+} showed a 10 cm^{-1} shift in the amide I mode, corresponding to loss of ordered structure at the A/W interface. In both the bulk phase and IRRAS experiments, protection against H→D exchange in AxV was enhanced only in the ternary complex. The combined data suggest that the secondary structure of AxV is strongly affected by the Ca^{2+}/membrane component of the ternary complex whereas lipid conformational order is unchanged by protein.

AxV[1] is a member of a family of structurally related, eukaryotic proteins that bind phospholipids in a calcium-dependent manner. Although these molecules have been implicated in a variety of membrane-related processes including membrane trafficking, signal transduction, anti-inflammatory activity, and blood coagulation (*1, 2*), their definitive in vivo functions have yet to be elucidated. Several detailed reviews have appeared (*3*−*6*).

AxV has been widely studied in terms of structure and membrane interactions. Its three-dimensional X-ray structure has been determined at atomic resolution (*7, 8*). AxV is a 33 kDa peptide composed primarily of α-helical secondary structure, with no apparent β-sheet. The molecule consists of 4 core domains of ∼70 residues each. Each of the domains exists as a four-helix bundle with a fifth "capping" helix crossing over the top. The four domains are organized symmetrically in a cyclical array, so that the axes of the α-helical bundles lie approximately perpendicular to the plane of the membrane. Ca^{2+} binding sites are located in interhelical loops at the interfacial surface. Cryoelectron microscopy studies of 2-D AxV crystals in contact with lipid monolayers have led to insights as to protein structural changes on membrane binding (*9, 10*). The affinity of AxV for anionic phospholipid membranes is in the nanomolar range in the presence of Ca^{2+} and negligible in the absence of the cation. The bulk of the evidence for AxV−membrane interaction is consistent with that of a peripheral protein bridged by Ca^{2+} ions (*11*).

Two recent spectroscopic studies have investigated the changes in membrane properties induced by calcium-dependent annexin binding in some detail. The effect of protein binding on the structure of mixed PC/PS vesicles and oriented bilayers was studied by fluorescence and NMR techniques (*12*). The presence of AxV led to the appearance of slow motions on the NMR time scale, indicating a reduction in the lipid diffusion rate. The advantages of using a lipid monolayer model for studying AxV interactions with phospholipids and Ca^{2+} were demonstrated in a recent joint study from our laboratories (*13*). Three techniques capable of providing information from monolayers at the A/W interface, namely, surface pressure (π), BAM, and IRRAS, were utilized to study the temporal, spatial, and structural organization of monolayers as a function of AxV and Ca^{2+}. The specific ternary interaction between AxV, DMPA, and

† This work was supported through U.S. Public Health Service Grants GM-29864 and GM-44554 to Rutgers University and to Boston University, respectively.

* Corresponding author. Telephone: (973) 353−5613. FAX: (973) 353−1264. E-Mail: mendelso@andromeda.rutgers.edu.

‡ Rutgers University.

§ Boston University School of Medicine.

[1] Abbreviations: A/W, air/water; AxV, annexin V; BAM, Brewster angle microscopy; DMPA, 1,2-dimyristoyl-*sn*-glycero-3-phosphatidic acid; DMPA-d_{54}, acyl-chain-perdeuterated DMPA; DOPC, 1,2-dioleoyl-*sn*-glycero-3-phosphocholine; EDTA, ethylenediaminetetraacetate; EGTA, ethylene glycol bis(β-aminoethyl ether)-*N*,*N*,*N*′,*N*′-tetraacetate; HEPES, *N*-(2-hydroxyethyl)piperazine-*N*′-2-ethanesulfonic acid hemisodium salt; IR, infrared; IRRAS, infrared reflection−absorption spectroscopy; LC, liquid condensed; LE, liquid expanded; NMR, nuclear magnetic resonance; POPS, 1-palmitoyl-2-oleoyl-*sn*-3-phospho-L-serine sodium salt; PC, phosphatidylcholine; PE, phosphatidylethanolamine; PS, phosphatidylserine; $\nu_s(CH_2)$, symmetric methylene stretching frequency; $\nu_{as}(CD_2)$, asymmetric methylene CD_2 stretching frequency.

10.1021/bi9819677 CCC: $18.00
Published on Web 12/17/1998

Ca^{2+} produced characteristic domain shapes and textures on an aqueous subphase. In particular, a marked rigidification of the monolayer was an effect produced solely by the protein/lipid/Ca^{2+} ternary complex.

The present study was undertaken to address two major issues: first, to determine the protein stability as a function of membrane binding; and second, to compare AxV secondary structure in bulk vs monolayer phases. These concerns have been addressed with bulk phase IR measurements of the thermal denaturation of AxV in its free and membrane-bound states, as well as by IRRAS studies of protein secondary structure in situ at the A/W interface. In addition to evaluating protein structural parameters, IR provides a convenient means for detecting any concomitant changes in lipid conformational order and phase behavior. The availability of IRRAS to monitor protein secondary structure in situ at the A/W interface offers substantial advantages for studying the interactions of extrinsic proteins with lipid environments.

MATERIALS AND METHODS

Materials. DMPA, DMPA-d_{54}, POPS, and DOPC were obtained from Avanti Polar Lipids (Alabaster, AL). HPLC-grade H_2O, chloroform, and methanol were all purchased from Fisher Scientific (Pittsburgh, PA). D_2O with 99.9% isotopic enrichment was supplied by Isotec (Miamisburg, OH). All other chemicals were obtained from Sigma (St. Louis, MO) and were of the highest purity commercially available.

Sample Preparation and IR Bulk Phase Experimental Methods. Recombinant rat AxV was prepared as described previously(*14*). AxV samples were stored in buffer A (50 mM HEPES, 100 mM KCl, 0.02% NaN_3, and 50 μM EGTA, pH 7.4) at 4 °C. The typical protein sample concentration was ~0.2 mM as determined by the Bradford assay. For bulk phase measurements of AxV thermal denaturation in D_2O solutions or membrane suspensions, 100 μL of the AxV stock solution was diluted with D_2O buffer A (pD 7.4) to 2 mL in an Amicon Centricon-10 concentrator (Beverly, MA). Three cycles of diluting and spinning in a Beckman JA-14 rotor (Fullerton, CA) at 5000 rpm (4 °C) yielded an AxV sample (in D_2O buffer A) at satisfactory concentrations for IR bulk phase measurements. The final filtrate was used for background subtraction. For experiments performed in the presence of Ca^{2+}, buffer A included 1 mM Ca^{2+}.

Bulk phase FTIR spectra were collected on a Mattson Instruments Research Series (RS-1) spectrometer equipped with an MCT detector and a sample shuttle. The spectrometer was under constant dry air purge. Multilamellar lipid vesicles were prepared by rehydration of a vacuum-dried lipid film with buffer A or protein solution. The lipid:protein molar ratio was 100:1. Samples for FTIR were placed between CaF_2 windows separated with a 25 μm spacer. A thermostated transmission cell (Harrick Scientific, Ossining, NY) was used together with a circulating water bath for temperature control. Temperatures were monitored with a digital thermocouple (Physitemp Instruments, Clifton, NJ) accurate to ±0.1 °C. All aqueous sample spectra were obtained at 4 cm^{-1} resolution by co-addition of 1024 interferograms. The interferograms were apodized with a triangular function and Fourier-transformed with two levels of zero-filling, yielding spectra encoded every ~1 cm^{-1}. For D_2O experiments, 8 blocks of 64 scans of sample and air background were co-added into separate files and ratioed to produce IR spectra with optimal water vapor compensation.

IRRAS Measurements. Our experimental setup has been described in detail (*15*) previously. Briefly, the angle of incidence was set to 35°, and unpolarized radiation was used. An optical filter (OFC Corp., Natick, MA) was positioned in the incident light path to reduce possible heating effects of the IR beam (*16*). A total of 1024 scans acquired with a resolution of 4 cm^{-1} were co-added and fast-Fourier-transformed with one level of zero-filling to yield spectra encoded every 2 cm^{-1}. A subphase of 100 mM NaCl and 2 μM EDTA in HPLC-grade H_2O (pH ~5.6) was used for DMPA compression experiments. A D_2O subphase of the same composition was employed for AxV injection measurements. The temperature of the subphase was controlled at 21 ± 0.5 °C with a circulating water bath. The monolayer was discontinuously compressed over a time period of 3 h. After the lipid LE/LC transition region was entered as monitored by surface pressure, the monolayer was allowed to relax for at least 10 min prior to protein injection. For film-free injections, the barrier was positioned at an area equivalent to the onset of LE/LC transition. The acquisition time for one spectrum was ~8 min. It took 4−5 h to complete a typical injection experiment. Each experiment was reproduced several times, and typical results are presented in this report. The final concentration of AxV in the subphase was ~0.06 μM, and that of Ca^{2+} was ~10 μM. The details of sample injection protocols have been described elsewhere (*13*).

IR Data Reduction Protocols. The precise values of $\nu_s(CH_2)$, $\nu_{as}(CD_2)$, and components of the protein amide I contour for the bulk phase experiments were determined from second-derivative spectra using software provided by the National Research Council of Canada. The peak position of the amide I contour was picked directly from the subtracted IR or IRRAS spectra using the same software. Spectral subtraction and baseline leveling were carried out with Grams/32 (Galactic Industries Corp., Ithaca, NY). Intensities of 1617 and 1650 cm^{-1} bands were obtained as peak heights from baseline leveled amide I envelopes.

Since the D_2O buffer exchange process was not 100% complete, a matching D_2O buffer background at the same temperature was subtracted from the protein spectra for evaluation of the amide I contour in the IR bulk phase measurements. The criteria for success of this operation is to match the residual H_2O and HOD contents of the sample and background spectra, as judged by the intensities of their respective stretching bands centered at ~3850 and 3420 cm^{-1} (*17*) and by the intensity of the HOD bending mode at ~1460 cm^{-1}. The last filtrate from the buffer exchange protocol worked well for this purpose, yielding a level baseline from ~3000 to ~1200 cm^{-1}. For experiments with PS vesicles, spectra of a pure lipid sample at the same concentration as the lipid−protein mixture were used for subtraction instead of the D_2O buffer. Contributions of the PS headgroup carboxylate at ~1620 cm^{-1} were subtracted from the protein amide I contour. The process was monitored by the disappearance of the PS carbonyl band centered at ~1750 cm^{-1}.

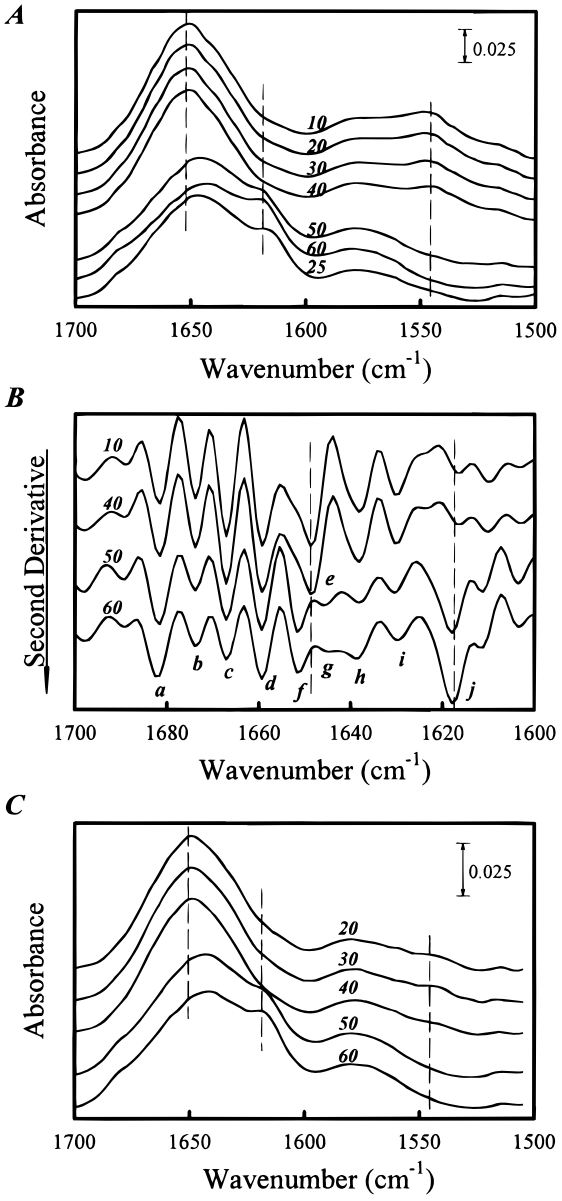

FIGURE 1: (A) IR spectra of the amide I and II spectral regions for pure AxV (buffer A, D_2O, pD 7.4) as a function of temperature (10−60 °C). The vertical dashed lines mark the main amide I band at ∼1650 cm^{-1} and a noticeable shoulder arising above 40 °C at 1617 cm^{-1}. Amide II peak intensity, marked at ∼1540 cm^{-1}, decreases with increasing temperature. The temperature-dependent changes are mostly irreversible as indicated in the spectrum acquired at 25 °C from a sample that was preheated to 60 °C and then cooled. The arrow represents an intensity of 0.025 AU. (B) Second derivatives of IR spectra for the amide I region of pure AxV as a function of temperature (10−60 °C). At low temperatures, eight bands are present at 1682, 1674, 1667, 1659, 1649 (a−e), 1638, 1630, 1616 cm^{-1} (h−j), respectively. Above 40 °C, the 1649 cm^{-1} band (e) splits into two bands at 1651 and 1645 cm^{-1} (f, g). (C) IR spectra of the amide I and II regions for pure AxV (buffer A, D_2O, pD 9.5) as a function of temperature (20−60 °C). The arrow represents an intensity of 0.025 AU.

RESULTS

Bulk Phase AxV in Binary and Ternary Mixtures with Phospholipids and/or Ca^{2+}. Spectra of AxV in buffer A at several temperatures are shown in Figure 1A. The broad spectral feature at 1652 cm^{-1} with several underlying components, as evidenced by shoulders, arises from the amide I mode (mostly peptide bond C═O stretch). Assignment of amide I bands to particular secondary structures (1615−1685 cm^{-1}) is nontrivial in general but in this case can be correlated with the rat AxV crystal structure (*8*).

Second-derivative spectra (Figure 1B) at low temperatures exhibit eight major features in the amide I region: 1616, 1630, 1638, 1649, 1659, 1667, 1674, and 1682 cm^{-1}. The two bands at 1649 and 1659 cm^{-1} are commonly assigned to helical secondary structures. These bands evidently make the strongest contribution to the original spectral contour, consistent with the crystal structure. While we cannot make definitive band assignments for specific helices in AxV, the frequency of a prominent band in the second-derivative spectra (1659 cm^{-1}) is close to that generally observed for hydrophobic helices. Assignment of the low-frequency bands at 1638 and 1631 cm^{-1} is uncertain. Although β-sheets may absorb in this region, their absence in the crystal structure makes this assignment untenable. Recent studies (*18*) have suggested that exposed α-helices which can form H-bonds in addition to those required for the structure absorb in the 1630−1635 cm^{-1} spectral region. The assignment was also suggested for the (flexible) ends of helices or distorted 3_{10}-helices.

Evaluation of temperature-induced changes in the amide I contour is simplified by examination of the second-derivative spectra which are overlaid in Figure 1B. We note that although the process of derivation narrows the component bands of the amide I contour, thereby facilitating their identification, the relative intensities of the components in the derivative spectrum are related to the width of the bands in the original contour and not to their fractional areas. Thus, the relative intensities of bands in derivative spectra are not appropriate for quantitative analysis. Figure 1A shows that between 10 and 40 °C, the amide I band intensity diminishes slightly, a probable result of temperature-induced density changes. More substantive alterations in the amide I contour become evident at ∼50 °C. The band at 1649 cm^{-1} is replaced by two features at 1651 cm^{-1} and a weaker band at 1645 cm^{-1}. A weak feature at 1616 cm^{-1} becomes masked by an intense band at 1617 cm^{-1}, with a concomitant increase in intensity of a weak high-frequency shoulder near 1682 cm^{-1}. These latter two bands have been observed in several studies of thermal denaturation in proteins where they appear to be marker bands for thermal denaturation (*19*−*21*), and are suggested to arise from extended or β-sheet-like structures.

For a predominantly helical protein like AxV, the amide II band is expected near 1550 cm^{-1}. Because the vibration arises from mixed N−H in-plane bending and C−N stretching modes, its position shifts to 1450 cm^{-1} upon H→D exchange in the peptide bonds. In spectra of dried proteins, the intensity of the amide II band is normally at least half that of the amide I mode. Thus, the spectra of AxV at 10 °C are suggestive of partial exchange prior to the onset of IR data acquisition. The residual amide II band shows a different temperature dependence than the amide I vibration. A small decrease in amide II intensity occurs between 10 and 40 °C and is followed by nearly complete elimination of the band as temperature is increased to 50 °C. The temperature-dependent changes of amide I and II bands are irreversible as seen from the spectrum obtained after recooling (to 25 °C) a previously heated sample (Figure 1A, 25 °C trace) The broad feature near 1580 cm^{-1} in all protein spectra

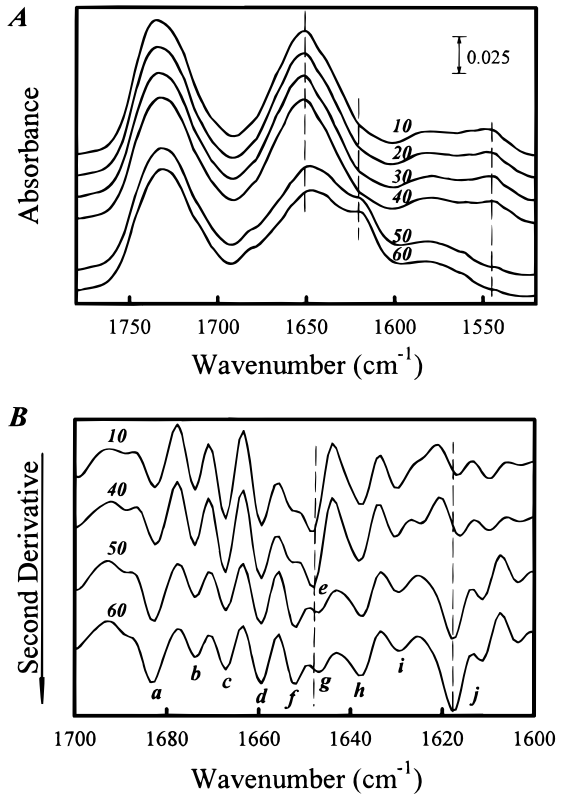

FIGURE 2: (A) IR spectra of Ca^{2+}-free AxV−DMPA/DOPC (buffer A, D_2O, pD 7.4) as a function of temperature (10−60 °C). The lipid carbonyl stretching mode is observed at ∼1735 cm^{-1}. The arrow represents an intensity of 0.025 AU. (B) Second derivatives of IR spectra for the amide I region of (A). The letters (a−j) represent the same peaks as in Figure 1B.

probably arises from protein side chains, e.g., carboxylate moieties, rather than amide II vibrations.

Spectra of AxV samples which were exchanged into D_2O buffer at pD 9.5 are shown in Figure 1C. The amide II band at 20 °C is less intense than that from the same temperature in Figure 1A, consistent with enhanced H→D exchange kinetics at higher pD. In contrast to amide II, however, the temperature dependence of the amide I region is unchanged from pD 7.4 to 9.5, indicating that the temperature-induced amide I spectral changes reflect conformational alterations rather than exchange phenomena.

Binary mixtures of AxV with acidic phospholipid-containing mixtures such as DMPA/DOPC and POPS/DOPC, in the absence of Ca^{2+}, produce spectral alterations similar to those observed for the pure protein as a function of temperature. The data for DMPA/DOPC/AxV in a Ca^{2+}-free buffer are shown in Figure 2A,B. The lipid carbonyl stretching mode is observed at ∼1735 cm^{-1}.

The remarkable stabilization of the AxV structure in a ternary complex of phospholipid/AxV/Ca^{2+} is evident from data shown in Figure 3A (raw absorbance) and Figure 3B (second derivative). AxV structure in DMPA/DOPC/AxV/Ca^{2+} vesicles shows much less evidence of thermal denaturation than in the Ca^{2+}-free binary system or in pure AxV solutions. In Figure 3A, the intensity (at 60 °C) of the low-frequency marker band at 1617 cm^{-1} is much reduced compared with Figures 1A or 2A. In addition, the main peak at ∼1650 cm^{-1} is much less altered at high temperature, with no apparent frequency shift. Examination of the derivative

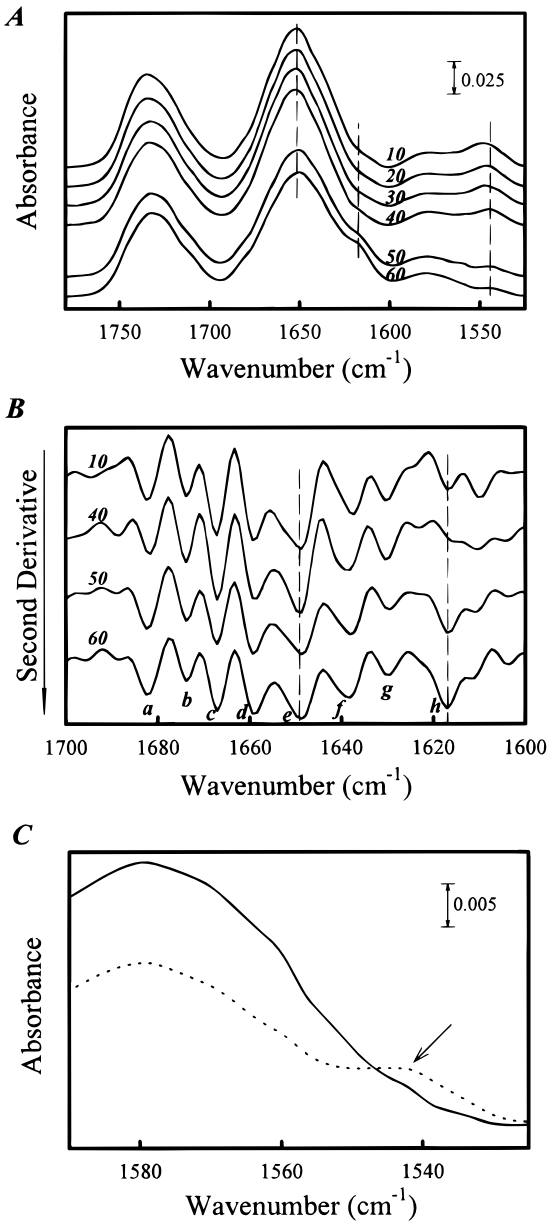

FIGURE 3: (A) IR spectra of AxV−DMPA/DOPC−Ca^{2+} (1 mM) in buffer A (D_2O, pD 7.4) as a function of temperature (10−60 °C). The lipid carbonyl stretching mode is observed at ∼1735 cm^{-1}. The main peak of the amide I band is marked at 1650 cm^{-1}, and the increase in intensity of the shoulder at 1617 cm^{-1} is not as strong as in Figures 1A and 2A. The arrow represents an intensity of 0.025 AU. (B) Second derivatives of IR spectra for the amide I region in (A). The band positions (a−e) are the same as in Figure 1B, while f−h are shown as h−j in Figure 1B. (C) 1590−1525 cm^{-1} region of AxV (solid line) and AxV−DMPA/DOPC−Ca^{2+} (dashed line) IR spectra at 60 °C. A residual amide II component at ∼1542 cm^{-1} is visible in the ternary system spectrum (arrow marked). The higher band intensity at ∼1580 cm^{-1} in the AxV spectrum is due to the more intense marker band at 1617 cm^{-1} in the spectrum of pure protein at 60 °C (Figure 1A).

spectrum confirms the Ca^{2+}-induced stabilization of the structure. There is little or no change in the amide I band pattern on heating except for the appearance of the marker band at 1617 cm^{-1}. Furthermore, there are no shifts in the α-helical bands or in the splitting of the 1649 cm^{-1} peak as a function of temperature.

The amide II region (1520−1560 cm^{-1}) may also serve as a useful marker of structural stability. In the current

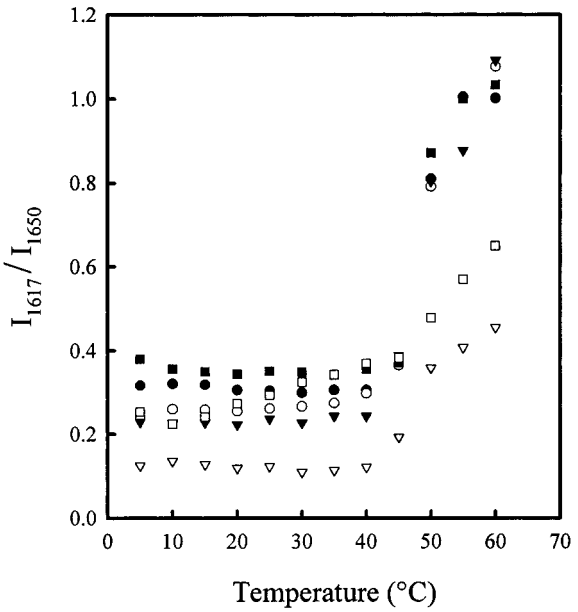

FIGURE 4: Relative intensities of 1617 and 1650 cm^{-1} bands (I_{1617}/I_{1650}) for various AxV samples plotted as a function of temperature. AxV (●), AxV−Ca^{2+} (○), AxV−DMPA/DOPC (▼), AxV−DMPA/DOPC−Ca^{2+} (▽), AxV−POPS/DOPC (■), and AxV−POPS/DOPC−Ca^{2+} (□) results are shown. Buffer A (D_2O, pD 7.4) and a Ca^{2+} concentration of 1 mM were used.

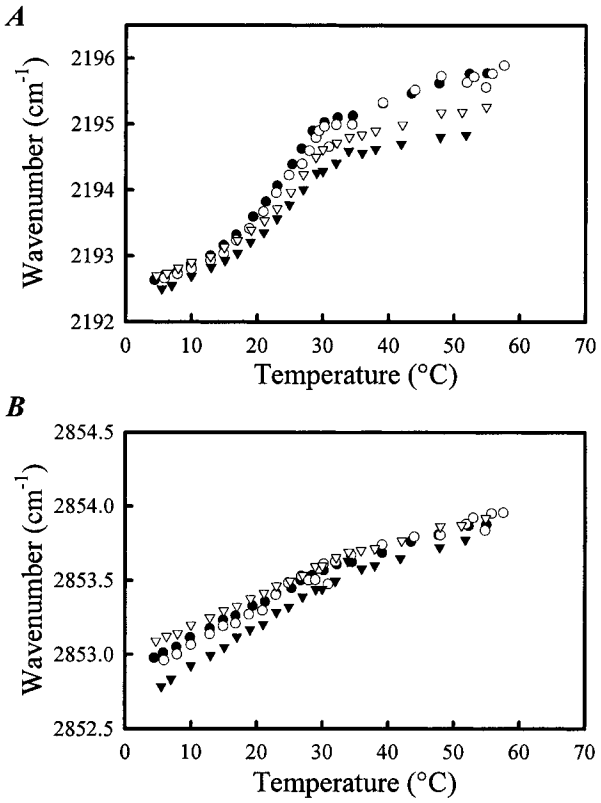

FIGURE 5: (A) $\nu_{as}(CD_2)$ are plotted as a function of temperature for DMPA-d_{54}/DOPC (●), DMPA-d_{54}/DOPC−Ca^{2+} (○), AxV−DMPA-d_{54}/DOPC (▼), and AxV−DMPA-d_{54}/DOPC−Ca^{2+} (▽) in buffer A. The Ca^{2+} concentration was 1 mM. (B) $\nu_s(CH_2)$ are plotted as function of temperature for the same samples and conditions as in (A).

experiments, AxV structure stabilization in ternary complexes is also evident from the amide II spectral region. In Figure 3C, this region is plotted for AxV alone and for an AxV/DMPA/DOPC/Ca^{2+} complex at 60 °C. Although the differences are small and the influence of the 1617 cm^{-1} marker band at high temperature is unavoidable, residual amide II intensity is evident as a weak feature at ∼1542 cm^{-1} only in the ternary complex. This protection against exchange is further evidence of a Ca^{2+}/phospholipid stabilization against temperature-induced perturbations in the AxV native structure.

Other data support a substantial stabilization of the native AxV structure in the protein/Ca^{2+}/lipid ternary complex. Comparison of the intensities of marker bands associated with native AxV structure (1650 cm^{-1}) or thermally denatured structure (1617 cm^{-1}) provides a measure of relative protein structure stabilization. To present these data more quantitatively, the 1617/1650 cm^{-1} peak height ratio is plotted in Figure 4 as a function of temperature for a series of relevant samples. The ternary complex samples (AxV + Ca^{2+} + DMPA/DOPC or POPS/DOPC) show a smaller change in 1617/1650 cm^{-1} intensity ratio index, compared with Ca^{2+}-free binary mixtures (AxV+lipid) or pure AxV samples. At 60 °C, the index ratio is ≤0.6 for the ternary complexes but >1.0 for other samples.

Bulk Phase Pure Phospholipid or Mixed Vesicles. The bulk phase transition characteristics of DMPA-d_{54}/DOPC 1:1 mixtures are shown in Figure 5A,B, as monitored by the temperature dependence of $\nu_{as}(CD_2)$ and $\nu_s(CH_2)$, respectively. The measured positions of these bands provide information about acyl chain conformational order, higher frequencies being indicative of a greater fraction of gauche bonds. The gel→liquid-crystal phase transition is at ≈52 °C for DMPA-d_{54} as determined from $\nu_{as}(CD_2)$ (data not shown). Addition of 1 mM Ca^{2+} has a strong ordering effect on pure DMPA-d_{54}, and results in the near-abolition of the transition. In the mixed lipid system (Figure 5A), the DMPA component exhibits a broadened melting process that is centered at 24 °C with a range of ∼12−29 °C (the actual onset of melting is difficult to estimate). The thermotropic behavior of the DOPC component in binary DMPA-d_{54}/DOPC lipid mixtures is shown in Figure 5B. As expected, the unsaturated and highly disordered acyl chains in this zwitterionic molecule do not show cooperative melting processes under our various experimental conditions (note the expanded vertical scale). The absence of a discernible transition is consistent with highly nonideal mixing or phase separation of these two lipids.

Addition of Ca^{2+} (1mM), AxV, or AxV/Ca^{2+} to the mixed lipid vesicles leaves the phase transition temperature essentially unchanged (Figure 5A). However, the slight (<1 cm^{-1}) lowering of $\nu_{as}(CD_2)$ upon addition of AxV and AxV/Ca^{2+}, above the transition, does suggest some ordering of liquid crystalline DMPA induced by AxV or AxV/Ca^{2+}.

Structure and Stability of AxV in Situ in Langmuir Films. Figure 6 displays the time dependence for adsorption of AxV to a lipid-free aqueous surface. The rapid increase in surface pressure to ∼7.5 mN/m after injection of AxV followed by a gradual monotonic increase reveals the strong surface activity of this protein.

To evaluate the structure and stability of AxV in monolayer films, IRRAS measurements of AxV in the amide I region for the protein alone, with lipid, and with lipid and Ca^{2+} are displayed in Figure 7. Films of pure AxV and AxV/Ca^{2+} each show a broad amide I peak centered at ∼1640

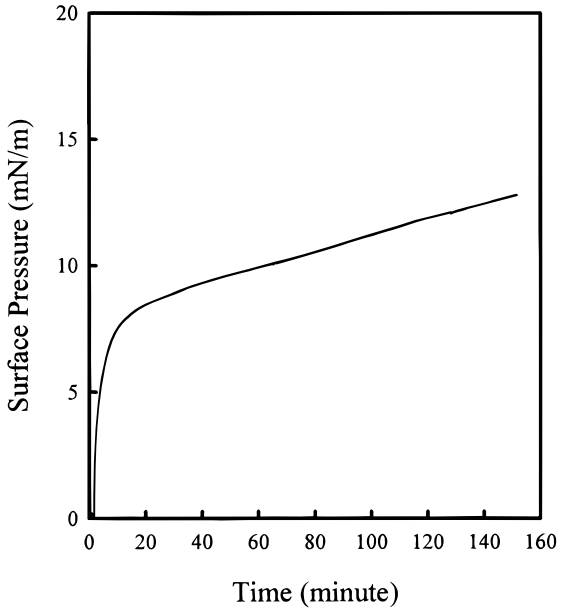

FIGURE 6: Surface pressure vs time after injection of AxV into a film-free subphase (100 mM NaCl, 2 μM EDTA, pH 5.6). The final protein concentration in the subphase was ~0.06 μM. The subphase temperature was 21 ± 0.5 °C.

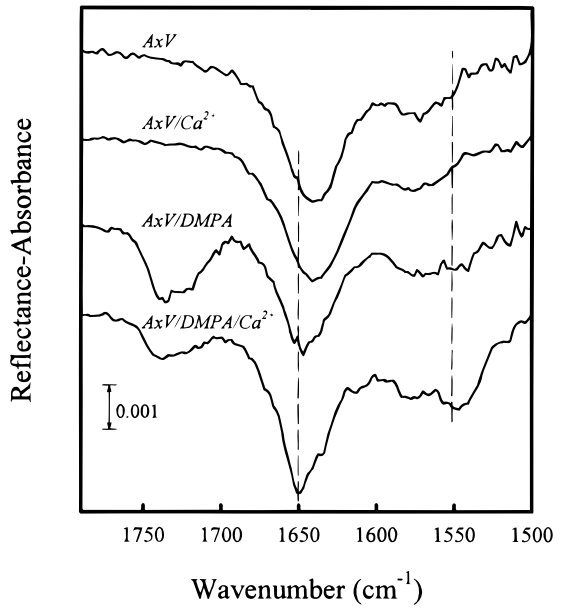

FIGURE 7: IRRAS spectra after injection of AxV or AxV/Ca^{2+} into a film-free or DMPA monolayer covered D_2O subphase (100 mM NaCl, 2 μM EDTA, pD 5.6) as indicated. The final concentrations of protein and Ca^{2+} were ~0.06 μM and ~10 μM, respectively. The subphase temperature was 21 ± 0.5 °C. Injections were made at the onset of the LE/LC phase transition of a DMPA monolayer or the equivalent surface area in the film-free cases. The vertical line marks the main amide I peak at ~1650 cm^{-1} observed in the presence of a DMPA monolayer compared with a band at ~1640 cm^{-1} without DMPA. The amide II peak is marked at 1550 cm^{-1}. The arrow represents a reflectance−absorbance intensity of 0.001.

cm^{-1}, shifted by 10 cm^{-1} to lower frequency from the AxV amide I mode in solution (Figure 1A). The large shift suggests a marked alteration in the secondary structure of AxV at the A/W interface. In contrast, AxV in lipid environments at the A/W interface, in both the presence and absence of Ca^{2+}, reveals an amide I frequency near the solution value of 1650 cm^{-1}. In the AxV/DMPA monolayer binary system, the amide I mode is shifted by 1−2 cm^{-1} to lower frequency compared to the AxV/Ca^{2+}/DMPA monolayer ternary system. The presence of residual water vapor and noise precludes the possibility of second-derivative (or other) analysis of the amide I contour in monolayers. However, the overall amide I band shape and peak positions in lipid monolayer environments are similar to those seen for all AxV samples, in the presence or absence of lipid, in the bulk phase at the same temperatures.

A second noteworthy feature of Figure 7 is the presence of a residual amide II band (marked in the figure with a vertical dashed line at 1550 cm^{-1}) observed only in the ternary monolayer system, similar to the bulk phase ternary system at lower temperatures. In samples without all three components (AxV, Ca^{2+}, and lipid), H→D exchange is almost complete in the D_2O environments as revealed by the absence of an amide II IRRAS peak.

DISCUSSION

Cellular functions of annexins are closely tied to their Ca^{2+}-dependent interactions with membrane lipids. There are several gaps in our current knowledge that the present work begins to address in terms of understanding structural and stability changes induced in both the protein and lipid components upon their mutual interaction. Previous studies have addressed these issues for the membrane lipids and report changes in parameters such as lateral diffusion rates (*12, 22*). Furthermore, AxV/Ca^{2+}/lipid ternary systems exhibit altered properties such as increased surface pressure, reduced curvature (*23, 24*), and increased rigidity (*13, 25*) that only occur with protein present. The essential role of the protein in these phenomena is not well understood.

The unique properties of the ternary system do not appear to arise from large-scale changes in protein conformation. Comparison of the AxV structure in soluble and membrane-bound forms by X-ray crystallography and high-resolution cryoelectron microscopy, respectively, reveals no major conformational differences other than a slight flattening of the molecule on the interfacial surface. Secondary structure differences between these forms are negligible as assessed by CD spectroscopy (*14, 26*). In terms of protein structure, the stabilization afforded by the ternary complex is most likely a consequence of the formation of crystalline arrays of AxV on the membrane suface. AxV forms trimers and extended trimer-based arrays on acidic phospholipid membrane surfaces, as demonstrated by chemical cross-linking (*27*) and cryoelectron microscopy studies (*9, 10*). The trimers lie along the surface of the lipid layer and crystallize in the lateral direction (*28*). These observations prompted the current investigation into other properties, such as thermal stability, of AxV as part of the ternary system.

The thermal properties of AxV have not been widely probed, except in its soluble form. Budisa et al. (*29*) have reported a melting temperature (T_m) of soluble AxV of 52 °C based on CD measurements at 222 nm. Light scattering measurements show that, at neutral pH, the protein begins to aggregate at around 60 °C (*30*), consistent with thermal denaturation. In CD studies of AxV, the presence of Ca^{2+} increases the melting temperature by ~3 °C, over the T_m of 58 °C for the Ca^{2+}-free form. Thermal unfolding is both

irreversible and highly cooperative (*31*). To our knowledge, thermal stability data have not been reported previously for membrane-bound AxV.

The current IR study of rat AxV provides additional information on the thermal stability of the ternary system, permitting detailed comparison between soluble and membrane-bound AxV and also between protein and lipid components. Absorbance and second-derivative data in Figures 1−3 reveal that in the absence of phospholipids, AxV denatures into a structure less ordered than wild-type, but retaining some elements of native protein structure. These elements are α-helical and probably correspond to the helical bundles that comprise much of the hydrophobic annexin core. Such a partially unfolded state is referred to as the "compact denatured" or "molten globule" state. From IR studies of thermal denaturation in other proteins, this physical state gives rise to marker bands near 1617 and 1682 cm^{-1}. Since these frequencies are usually associated with β-sheet structure, these marker bands have been attributed to intermolecular aggregation of extended polypeptides (*32*). Regardless of the structural interpretation, the appearance of these bands marks the onset of thermal denaturation/aggregation in AxV samples. The irreversibility of the process is clearly revealed from the IR spectrum (e.g., Figure 1A) of a sample heated to 60 °C and then cooled to 25 °C. The peak near 1617 cm^{-1} (Figure 1A) retained most of its intensity under these conditions. Although the melting temperature was not determined as precisely in the current study as in the work of Budisa et al. (*29*), our observed value for rat AxV in the absence of phospholipids (Figure 4) is 47 ± 1 °C. Besides the slight differences in the sequence of human compared to rat AxV, the difference in observed transition temperatures between the IR and CD measurements may reflect the higher concentrations required for the IR (6 mg/mL vs 0.08 mg/mL, respectively) and the fact that an aggregation-based denaturation as observed here will display a substantial concentration dependence (*33*).

In contrast to the marked increase in protein stability in the ternary complex, protein-induced perturbations of lipid structure are small. The effect of AxV on the PA component of DMPA-d_{54}/DOPC mixtures reveals no major changes in the thermotropic behavior of the deuterated component. A slight ordering in the DMPA component above its phase transition, in the presence of protein, is suggested from the reduction in frequency at temperatures above the completion of the melting process. This minor change is consistent with peripheral protein binding and with a recent study of Saurel et al. (*12*), who examined the consequences of AxV binding on the structure and dynamics of PC/PS bilayers using a variety of fluorescence and NMR-based experiments. They observed the appearance of slow motions (on the NMR time scale) in the lipid spectra, indicative of a decrease in lipid lateral diffusion, but observed no indication of changes in the lipid molecular packing and acyl chain flexibility in either of the lipid components. Their results suggest a fluid−fluid phase separation of PC into PC-rich and PC/PS domains, the latter thought to be associated with AxV. Both the study of Saurel et al. and an earlier investigation by Gilmanshin et al. (*22*) of annexin IV with POPG/POPC mixtures were consistent with the appearance of distinct protein-induced lipid regions.

The added dimension afforded by IR is that IRRAS measurements permit the direct evaluation of AxV secondary structure in monolayers at the A/W interface. The surface activity of AxV is indicated directly from the time course of surface pressure changes following AxV injection into an aqueous subphase. The rapid initial increase in surface pressure (Figure 6) is strong evidence for the surface activity of the recombinant rat AxV in contrast to earlier studies (*34*, *35*). The discrepancy between the results may be attributed to the use of different sources of annexin.

In IRRAS samples lacking a phospholipid monolayer, adsorption of AxV to the film-free subphase is accompanied by a substantial change in secondary structure. The 10 cm^{-1} shift in the amide I position from 1650 to 1640 cm^{-1} is typical of the formation of random coil and a loss of helical structure. This shift is consistent with large-scale unfolding or denaturation at the A/W interface, which commonly occurs with proteins. However, unlike the thermal denaturation, the structural change of AxV at A/W does not exhibit the ∼1615−1625 cm^{-1} marker band in the amide I contour, suggesting different mechanisms for the two processes. Adsorption of AxV is also accompanied by extensive H→D exchange, as revealed by essentially complete loss of the amide II intensity at 1550 cm^{-1}. Ca^{2+} does not protect against this surface denaturation, as similar effects are noted for AxV adsorbed to the surface of a Ca^{2+}-containing subphase.

The presence of DMPA monolayers in the IRRAS experiments changes the situation dramatically. For the ternary system, the amide I contour strongly resembles that of bulk phase AxV; in addition, the amide II/amide I relative intensities are similar to those of the bulk phase protein (compare Figure 7 with Figure 1A). Thus, AxV in the ternary system is protected from surface denaturation at the A/W interface. For AxV adsorbed to the DMPA monolayer in a Ca^{2+}-free environment, a very small shift to lower frequency is noted in the amide I mode, while a slight residual intensity at 1550 cm^{-1} indicates that H→D exchange is not as extensive as in the lipid-free films. However, H→D exchange is more extensive in the Ca^{2+}-free DMPA monolayer system than for the ternary system. Our previous study revealed the lack of a specific interaction between AxV and DMPA monolayers (*13*). The protein simply adsorbs to the aqueous surface, limiting the surface area available to the lipid molecules and forcing them from gaseous or LE phases into LC domains. This nonspecific adsorption of AxV is sufficient to maintain an almost-native protein structure. In contrast, participation in the ternary complex offers further structural stabilization and limits solvent accessibility to the peptide bonds, as indicated by residual amide II intensity.

In conclusion, formation of the AxV/Ca^{2+}/lipid ternary complexes, either in bulk or in monolayer phases, stabilizes AxV structure and protects against thermal denaturation and some degree of H→D exchange. Nonspecific adsorption to lipid monolayers did not promote the same protection against H→D exchange. Though previous CD data have suggested that addition of Ca^{2+} tends to stabilize the overall AxV structure (*36*), the present data indicate that the cation alone has much less effect on AxV thermostability or H→D exchange properties than do Ca^{2+} and phospholipid. The enhanced stability associated with the AxV ternary complex is similar to that induced by high-affinity binding of ligands to other proteins. For example, the addition of biotin to

streptavidin increases its thermostability from 75 to 112 °C (*37*).

Finally, it is notable that the protein and lipid components show marked differences in the degree of structural stability afforded by ternary complex formation. The AxV component is strongly influenced, whereas lipid structure is at most slightly altered.

REFERENCES

1. Donnelly, S. R., and Moss, S. E. (1997) *Cell. Mol. Life Sci. 53*, 533−538.
2. Reutelingsperger, C. P. M., and Vanheerde, W. L. (1997) *Cell. Mol. Life Sci. 53*, 527−532.
3. Swairjo, M. A., and Seaton, B. A. (1994) *Annu. Rev. Biophys. Biomol. Struct. 23*, 193−213.
4. Raynal, P., and Pollard, H. B. (1994) *Biochim. Biophys. Acta 1197*, 63−93.
5. Seaton, B. A. (1996) *Annexins: Molecular Structure to Cellular Function*, 1st ed., R. G. Landes Company, Austin, TX.
6. Gerke, V., and Moss, S. E. (1997) *Biochim. Biophys. Acta 1357*, 129−154.
7. Huber, R., Romisch, J., and Paques, E. P. (1990) *EMBO J. 9*, 3867−3874.
8. Concha, N. O., Head, J. F., Kaetzel, M. A., Dedman, J. R., and Seaton, B. A. (1993) *Science 261*, 1321−1324.
9. Olofsson, A., Mallouh, V., and Brisson, A. (1994) *J. Struct. Biol. 113*, 199−205.
10. Voges, D., Berendes, R., Burger, A., Demange, P., Baumeister, W., and Huber, R. (1994) *J. Mol. Biol. 238*, 199−213.
11. Swairjo, M. A., Concha, N. O., Kaetzel, M. A., Dedman, J. R., and Seaton, B. A. (1995) *Nat. Struct. Biol. 2*, 968−974.
12. Saurel, O., Cezanne, L., Milon, A., Tocanne, J. F., and Demange, P. (1998) *Biochemistry 37*, 1403−1410.
13. Wu, F., Gericke, A., Flach, C. R., Mealy, T. R., Seaton, B. A., and Mendelsohn, R. (1998) *Biophys. J. 74*, 3278−3281.
14. Swairjo, M. A., Roberts, M. F., Campos, M. B., Dedman, J. R., and Seaton, B. A. (1994) *Biochemistry 33*, 10944−10950.
15. Flach, C. R., Prendergast, F. G., and Mendelsohn, R. (1996) *Biophys. J. 70*, 539−546.
16. Sakai, H., and Umemura, J. (1997) *Langmuir 13*, 502−505.
17. Gericke, A., Smith, E. R., Moore, D. J., Mendelsohn, R., and Storch, J. (1997) *Biochemistry 36*, 8311−8317.
18. Gilmanshin, R., Williams, S., Callender, R. H., Woodruff, W. H., and Dyer, R. B. (1997) *Biochemistry 36*, 15006−15012.
19. Muga, A., Arrondo, J. L., Bellon, T., Sancho, J., and Bernabeu, C. (1993) *Arch. Biochem. Biophys. 300*, 451−457.
20. Martínez, A., Haavik, J., Flatmark, T., Arrondo, J. L. R., and Muga, A. (1996) *J. Biol. Chem. 271*, 19737−19742.
21. Medrano, F. J., Gasset, M., López-Zúmel, C., Usobiaga, P., Garcia, J. L., and Menéndez, M. (1996) *J. Biol. Chem. 271*, 29152−29161.
22. Gilmanshin, R., Creutz, C. E., and Tamm, L. K. (1994) *Biochemistry 33*, 8225−8232.
23. Andree, H. A., Stuart, M. C., Hermens, W. T., Reutelingsperger, C. P., Hemker, H. C., Frederik, P. M., and Willems, G. M. (1992) *J. Biol. Chem. 267*, 17907−17912.
24. Swairjo, M. A., Seaton, B. A., and Roberts, M. F. (1994) *Biochim. Biophys. Acta 1191*, 354−361.
25. Vénien-Bryan, C., Lenne, P. F., Zakri, C., Renault, A., Brisson, A., Legrand, J. F., and Berge, B. (1998) *Biophys. J. 74*, 2649−2657.
26. Plager, D. A., and Nelsestuen, G. L. (1994) *Biochemistry 33*, 13239−13249.
27. Concha, N. O., Head, J. F., Kaetzel, M. A., Dedman, J. R., and Seaton, B. A. (1992) *FEBS Lett. 314*, 159−162.
28. Reviakine, I., Bergsmaschutter, W., and Brisson, A. (1998) *J. Struct. Biol. 121*, 356−362.
29. Budisa, N., Minks, C., Medrano, F. J., Lutz, J., Huber, R., and Moroder, L. (1998) *Proc. Natl. Acad. Sci. U.S.A. 95*, 455−459.
30. Beermann ofm cap, B. B., Hinz, H. J., Hofmann, A., and Huber, R. (1998) *FEBS Lett. 423*, 265−269.
31. Arboledas, D., Olmo, N., Lizarbe, M. A., and Turnay, J. (1997) *FEBS Lett. 416*, 217−220.
32. van Stokkum, I. H. M., Linsdell, H., Hadden, J. M., Haris, P. I., Chapman, D., and Bloemendal, M. (1995) *Biochemistry 34*, 10508−10518.
33. Creighton, T. E. (1992) *Protein Folding*, W. H. Freeman and Company, New York.
34. Mukhopadhyay, S., and Cho, W. (1996) *Biochim. Biophys. Acta 1279*, 58−62.
35. Bandorowicz-Pikula, J., Sikorski, A. F., Bialkowska, K., and Sobota, A. (1996) *Mol. Membr. Biol. 13*, 241−250.
36. Sopkova, J., Gallay, J., Vincent, M., Pancoska, P., and Lewit-Bentley, A. (1994) *Biochemistry 33*, 4490−4499.
37. González, M., Bagatolli, L. A., Echabe, I., Arrondo, J. L. R., Argaraña, C. E., Cantor, C. R., and Fidelio, G. D. (1997) *J. Biol. Chem. 272*, 11288−11294.

BI9819677